Journal of Sound and Vibration (1997) **204**(1), 99–116

THE INFLUENCE OF IMPERFECTIONS ON THE EIGENFREQUENCIES OF A ROTATING COMPOSITE SHAFT

H. L. WETTERGREN

Department of Mechanical Engineering, Linköping University, 58183 *Linköping, Sweden*

(*Received* 28 *May* 1996, *and in final form* 20 *January* 1997)

The influence of imperfections of a rotating composite shaft is considered. When the shaft is non-rotating the geometry remains unchanged and the eigenfrequencies depend only on the material stiffness. In high speed applications the eigenfrequencies also depend on the new geometry. The difference between these two cases is negligible, which means that the change in the stiffness has much greater influence than the change in the geometry. The difference between the eigenfrequencies in the x and y directions, $\Delta\omega$, depends on the term used in a Fourier series expansion of the radius. The second cosine term is shown to have the largest influence on the eigenfrequencies and the dependence is almost linear. Imperfections of the types described in this paper have largest influence when the filament winding angle is about 60°.

1. INTRODUCTION

The behavior of composite shafts in rotordynamic applications have been investigated by Zorzi and Giordano [1] and Bauchau [2, 3], among others. Zorzi and Giordano showed that composite materials are potentially viable candidates for supercritical shafting. They showed that composite shaft performance is predictable, the expected critical speed can be achieved, and no classical rotordynamic instability problems occurred during their experiments. One major observation was that the composite shafts tested showed greater sensitivity to unbalance than the aluminium control shaft. Other practical experiences indicate that it is normally difficult to run simple composite shafts supercritically; instability often occurs. One explanation of this is, of course, the larger internal damping in composite materials compared to that in traditional rotor materials. This paper is concerned, however, with another difference: the possibility of having instabilities due to non-symmetric shaft geometry. To understand why this and other kinds of dynamic differences may occur between shafts made from composite material, compared to shafts made from conventional rotor material, requires knowledge of the manufacturing process.

In the filament winding process, continuous layers of reinforcement are built up by winding rovings or monofilaments over a mandrel. Filament-laying mechanisms synchronized with the rotation of the mandrel enable the winding angle and placement of the reinforcing material to be controlled, and the total thickness is built up from a number of layers wound at the same or different angles. Winding angles may vary from very small angles to ones almost perpendicular to the axis of the mandrel. The wound material is bound by a thermosetting resin, which may be applied during the winding process if the "wet winding" process is used.

0022–460X/97/260099 + 18 $25.00/0/sv970937

Usually, the filament-wound composite is cured at elevated temperatures without any additional compaction. Another possibility is to roll Mylar film around the wound shaft. The mandrel expands during curing and the Mylar film exerts sufficient pressure to squeeze out the excess resin. Curing can also be done in an autoclave.

This complicated manufacturing process may lead to imperfections in the shaft. According to the *Engineered Materials Handbook*, volume 1 [14], the three most common imperfections are as follows: void or porosity content—the volume of voids within a laminate may be up to 1–2%; resin content, fibre volume and associated distribution gradients may differ from what was intended; the wrong laminate geometry.

Normally, especially for thick or homogeneous shafts, differences in the behavior at different rotational speeds may not have to be considered. Due to dynamic forces, imperfections of thin shafts will, however, lead to changes in the geometry. This phenomenon arises for all types of materials. The filament winding process may lead to kinds of imperfections for rotors made from composite materials which are different from those for rotors made from steel/aluminum. Rotors made from composite material may also be used in applications where the rotational frequency is higher than for common rotors.

These imperfections can cause several effects on the behavior of the rotor. The two most important are as follows: mass unbalances—if the mass center moves from the rotation axis, an eccentricity is introduced which leads to centrifugal forces, an effect which is often the most important; different stiffnesses in different directions—if a rotor had different eigenfrequencies in the x and y directions and if no external damping acts on the rotor, the rotor will be unstable between these eigenfrequencies.

This paper is concerned with the effects due to the imperfections described above and their origin. To be able to describe these effects the radius obtained due to the imperfections, which is dependent of the circumferential position and the rotational speed, as $r = r(\theta, \Omega)$, has to be Fourier series expanded.

The arbitrary geometry of the cross-sectional area of the shaft is shown in Figure 1. The radius may be expressed as a Fourier series expansion as

$$r(\theta, \Omega) = R_0(\Omega) + \sum_{n=1}^{\infty} \Delta r_n(\Omega) \cos n\theta, \tag{1}$$

or sometimes in a more general form,

$$r(\theta, \Omega) = R_0(\Omega) + \sum_{n=1}^{\infty} (a_n(\Omega) \cos n\theta + b_n(\Omega) \sin n\theta). \tag{2}$$

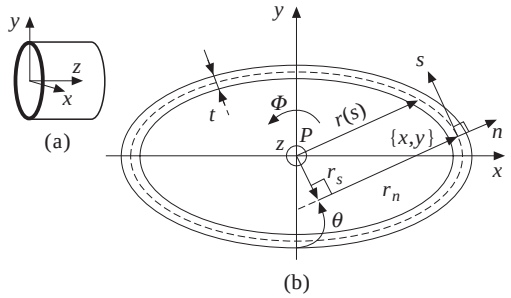

Figure 1. The cross-section geometry of the shaft.

In this Fourier series expansion of the radius the origin of the following effects can be seen. The change in R_0 leads to changes in the eigenfrequencies. The first cosine term moves the mass center from the rotational axis, which leads to increasing centrifugal forces but does not affect the eigenfrequencies. The second cosine term leads to different stiffnesses in different directions. Only the terms with values of n equal to 3 and 4 influence eigenfrequencies significantly.

In this study attention has been focused on the difference in the behavior of the eigenfrequencies of a cylindrical shaft due to delamination in a region of different size and different position. A comparison between differences in the eigenfrequencies due to delamination and other types of imperfections is also made.

2. FE FORMULATION

In the analyses a special developed FE program with a ten-degree-of-freedom thin-walled finite element for laminate composite beams, developed by Wu and Sun [5], has been used. Their element, here called the WS element, was further developed and extended by Wettergren [6]. The element allows transverse shear, warping and, moreover, the mass is not distributed on the centerline of the beam. This means that gyroscopic effects are included in the analyses. However, their contribution to the results in this paper can be neglected. Section 2.1 is a short summary of reference [5].

2.1. THE WS ELEMENT

Let (x, y, z) be a fixed Cartesian co-ordinate system (see Figure 1(a)), with axis parallel to the axis of the beam. The length of the element is h. The plane normal to the longitudinal axis z cuts the middle surface of the beam cross-section along the curved line, called the contour; see Figure 1(b). A local contour co-ordinate system (n, s, z) is placed on the middle surface, where n and s are the normal and tangential directions to the contour, respectively.

To derive the finite element for a laminated composite thin-walled beam, three assumptions were made as follows.

(1) The contour does not deform in its own plane. This assumption leads to the displacement of a point on the middle surface u, v in the x and y directions, respectively, being expressible as

$$u(s, z) = U(z) \sin \theta(s) - V(z) \cos \theta(s) - \Phi(z) r_s(s), \tag{3}$$

$$v(s, z) = U(z) \cos \theta(s) + V(z) \sin \theta(s) + \Phi(z) r_n(s), \tag{4}$$

where U and V are the displacements of the pole P in the x and y directions, respectively, and Φ is the rotation angle around the pole axis. The other variables are defined in Figure 1.

(2) The Saint-Venant assumption of the deformation of a twisted shaft is valid. Saint-Venant assumes that the deformation of the twisted shaft consists of rotations of cross-sections of the shaft, as in the case of a circular shaft, and of warping of the cross-sections, which is the same for all cross-sections. This leads to the axial displacement w on the contour being expressible as

$$w(s, z) = W(z) + \xi(z) x(s) + \eta(z) y(s) + \Psi(z) \omega(s), \tag{5}$$

where W is the average displacement of the beam in the z direction. In the classical theory of thin-walled beams, $\xi = -U'$, $\eta = -V'$, $\theta = \Phi'$ and ω is the warping function.

(3) The Kirchhoff–Love assumption in classical shell theory remains valid for thin-walled composite beams. This means that the strains off the middle surface are given by

$$\varepsilon_s = \frac{\varepsilon_{s0} - \zeta\chi_s}{1 + \zeta/a}, \qquad \varepsilon_z = \varepsilon_{z0} - \zeta\chi_z, \tag{6, 7}$$

$$\gamma_{sz} = (\mu_{zs} - \zeta\varkappa_{zs})/(1 + \zeta/a) + \mu_{sz} - \zeta\varkappa_{sz}, \tag{8}$$

where the unit strains of the middle surface are given by

$$\varepsilon_{z0} = \partial w/\partial z, \qquad \varepsilon_{s0} = \partial v/\partial s + u/a. \tag{9, 10}$$

The shearing strains are given by

$$\mu_{sz} = \partial v/\partial z, \qquad \mu_{zs} = \partial w/\partial s. \tag{11, 12}$$

The changes of curvature of the shell are given by

$$\chi_z = \partial u^2/\partial^2 z, \qquad \chi_s = (\partial/\partial s)(\partial u/\partial s - v/a). \tag{13, 14}$$

The twist of the shell is given by

$$\varkappa_{sz} = (\partial/\partial z)(\partial u/\partial s - v/a), \qquad \varkappa_{zs} = \partial u^2/\partial z\,\partial s. \tag{15, 16}$$

The variable $a(s)$ is the radius of curvature of the contour, defined to be positive when the center of the curvature lies on the negative n-axis (see Figure 1(b)).

The thickness of the wall of the laminated beams is built up of an arbitrary number of bonded orthotropic layers having different thicknesses and fiber orientations. The stresses and strains with respect to the structural principal axes n, s and z (see Figure 1(b)) in each layer are related by

$$\begin{Bmatrix} \sigma_z \\ \sigma_s \\ \tau_{zs} \end{Bmatrix} = \begin{bmatrix} \bar{Q}_{11} & \bar{Q}_{12} & \bar{Q}_{16} \\ \bar{Q}_{12} & \bar{Q}_{22} & \bar{Q}_{26} \\ \bar{Q}_{16} & \bar{Q}_{26} & \bar{Q}_{66} \end{bmatrix} \begin{Bmatrix} \varepsilon_z \\ \varepsilon_s \\ \gamma_{zs} \end{Bmatrix}, \tag{17}$$

where $\bar{Q}_{ij}$ are the reduced stiffnesses for the unidirectional fiber composite relative to the (n, s, z) co-ordinates.

The strain energy for each element is given by

$$U = \tfrac{1}{2}\{q\}^{\mathrm{T}}[K]\{q\}, \tag{18}$$

where $[K]$ is the element stiffness matrix, expressed as

$$[K] = \int_0^h [H]^{\mathrm{T}} \left(\int_0^S [B]^{\mathrm{T}}[S][B]\,\mathrm{d}s \right) [H]\,\mathrm{d}z \tag{19}$$

and

$$\{q\} = [W_1\ \xi_1\ \eta_1\ \Psi_1\ U_1\ V_1\ \Phi_1\ U_1'\ V_1'\ \Phi_1'\ W_2\ \xi_2\ \eta_2\ \Psi_2\ U_2\ V_2\ \Phi_2\ U_2'\ V_2'\ \Phi_2']^{\mathrm{T}}. \tag{20}$$

The kinetic energy for each element is given by

$$T = \tfrac{1}{2}\{\dot{q}\}^{\mathrm{T}}[M]\{\dot{q}\}, \tag{21}$$

where $[M]$ is the element mass matrix, expressed as

$$M = \int_0^h [H^*]^{\mathrm{T}} \left(\int_0^S [C]^{\mathrm{T}} \varrho t [C] \, \mathrm{d}s \right) [H^*] \, \mathrm{d}z. \tag{22}$$

By using the above-described FE formulation, the imperfections of concern in this paper may be studied.

3. EFFECTS FROM VARIATION IN THE RADIUS

The behavior of a rotor has been studied due to variation in the radius (see Figure 2).

To isolate the instability problem, only the beam-like frequencies will be studied. The behavior is compared with that predicted by basic Euler–Bernoulli beam theory, which gives the first non-zero eigenfrequency in the x direction for a freely supported beam as

$$\omega_x = (3{\cdot}5608 \times 2\pi/l^2)\sqrt{I_x E/A\rho}, \tag{23}$$

and in the y direction as

$$\omega_y = (3{\cdot}5608 \times 2\pi/l^2)\sqrt{I_y E/A\rho}, \tag{24}$$

where the moments of inertia are, in the x direction,

$$I_x = \int_A y^2 \, \mathrm{d}A, \tag{25}$$

and, in the y direction,

$$I_y = \int_A x^2 \, \mathrm{d}A. \tag{26}$$

The beam area may be calculated by the approximate expression

$$A = \int_S t(s) \, \mathrm{d}s. \tag{27}$$

A "simple" solution is obtained by using equations (25), (26) and (27) in equations (23) and (24). They give ω_e with basic beam theory (called the Euler–Bernoulli solution in Table 1). These simple solutions and finite element analyses with the WS element are presented in Table 1. In this table different values of n in

$$r = R_0 + \Delta r \cos n\theta \tag{28}$$

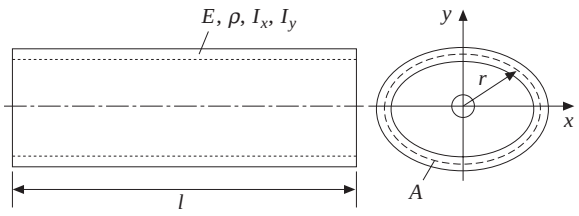

Figure 2. A free–free beam.

and different values of N in

$$r = R_0 + \sum_{n=2}^{N} \Delta r_n \cos n\theta \tag{29}$$

have been used. Every part of the table contains ω_x/ω_0 and ω_y/ω_0, where ω_0 is the eigenfrequency for the circular contour, given by equations (23) and (24) with I_x or I_y and A from equation (27). The eigenfrequencies for the non-rotating free–free beam, ω_x and ω_y, are the eigenfrequencies in the x and y directions, seen in Figure 2, for the contour with a circumferential radius variation ($r = r(\theta)$). The radius-to-length ratio, $R/l = 0{\cdot}05$, and the thickness to radius ratio, $t/R = 0{\cdot}04$, have been used for the calculation of the eigenfrequencies with 16 beam elements of a total length of the beam $l = 1$ m.

It is shown in Table 1 that the second term in the Fourier series, $n = 2$, has the largest influence on the difference between the eigenfrequency for the circular contour and the eigenfrequencies for the contour with a circumferential radius variation. The influence of terms with $n \geq 2$ can normally be neglected. When more than one term is included in the analyses, the difference from the result when $n = 2$ is negligible. The Euler–Bernoulli solution and the analysis with the WS element give almost the same results.

3.1. NON-LINEAR INFLUENCE DUE TO Δr_n

The linearity of the relation between ω and Δr has been studied for different terms in the Fourier series expansion. The aim is to see if all terms are affected in the same manner when Δr increases. The results are presented in Figure 3. From Figure 3 it is noted that when $n = 2$ the frequency ratio ω_y/ω_0 is almost proportional to the radius ratio $\Delta r_n/R$, but the influences on ω_y/ω_0 from the other terms increase more than linearly: however, their absolute values are normally negligible compared to that when $n = 2$.

4. CHANGES IN THE GEOMETRY DUE TO IMPERFECTIONS

Yurgartis [7] showed that continuous, non-woven fibres in high performance composites have small angular misalignments about their mean direction. The origins of fibre

TABLE 1

The influence of Δr_n and n on ω_x/ω_0 (upper value) and ω_y/ω_0 (lower value); $t/R_0 = 0{\cdot}04$ and $R_0/l = 0{\cdot}05$

	Euler–Bernoulli		WS element	
n	$\Delta r_n/R_0 = 0{\cdot}02$	$\Delta r_n/R_0 = 0{\cdot}04$	$\Delta r_n/R_0 = 0{\cdot}02$	$\Delta r_n/R_0 = 0{\cdot}04$
2	0·9850 1·0152	0·9706 1·0307	0·9872 1·0152	0·9747 1·0262
3	1·0001 1·0001	1·0001 1·0001	1·0003 1·0003	1·0010 1·0010
4	1·0001 1·0001	1·0001 1·0001	1·0001 1·0001	1·0010 1·0010
2, 3	0·9852 1·0164	0·9711 1·0354	0·9873 1·0134	0·9750 1·0265
2, 3, 4	0·9849 1·0174	0·9698 1·0395	0·9870 1·0144	0·9739 1·0316

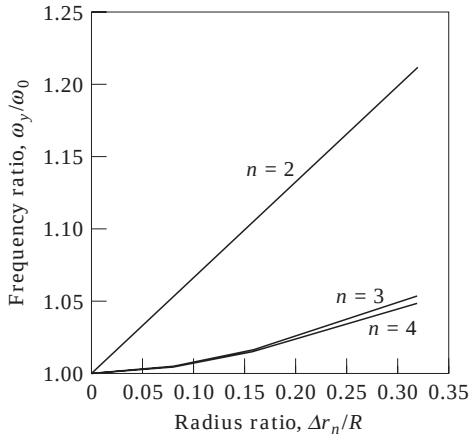

Figure 3. The influence of $\Delta r_n/R$ on ω_y/ω_0 for different values of n.

misorientations are still a matter of speculation. Nonetheless, the presence of angular misalignment has been recognized for many years. According to Yurgartis, fibre misalignment has been suspected of having a significant influence on composite properties such as longitudinal tensile modulus, longitudinal compression, strength and delamination fracture toughness among others.

Due to dynamic forces, imperfections of thin-walled shafts will lead to changes in the geometry. To see what kind of changes in the geometry these imperfections cause and to see how the eigenfrequency will be influenced, a thin circular beam with radius R has been studied. The beam with the lay-up $[(45^\circ, -45^\circ)_4]_{s16}$ has different filament winding angle over a certain part of the periphery, given by φ, symmetrically around the y-axis (see Figure 4).

The deformation of the beam due to dynamic forces has been analyzed with the FEM program ABAQUS. A total of 108 elements of the type S8R5 have been used to model the beam. S8R5 is a double curved Shell element with 8 nodes, Reduced integration, using 5 degrees of freedom per node. To avoid rigid body motion, weak elements have been used at the ends. The centers of the ends are fixed in both the x and y directions. The elements at the ends are so weak that the effect on the deformation of the contour of the shaft is negligible.

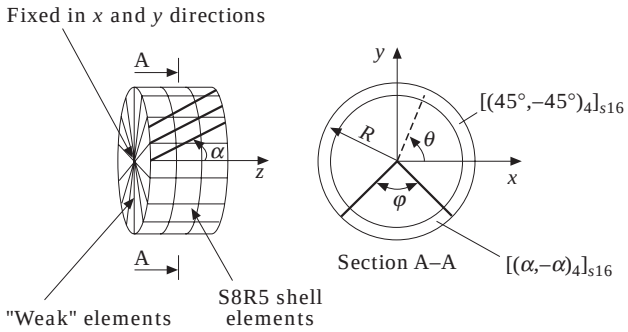

Figure 4. A composite beam with a different filament winding angle, α, over φ. The thickness-to-radius ratio (t/R) is 0·04. The middle radius, R, is equal to 0·05 m when $\Omega = 0$ rpm.

The resulting geometry may be represented by the Fourier series

$$R_0 + \sum_{n=1}^{\infty} (a_n \cos n\theta + b_n \sin n\theta), \tag{30}$$

where

$$a_n = \frac{2}{S}\int_0^S r(s) \cos \frac{n\pi s}{S}\, \mathrm{d}s, \qquad b_n = \frac{2}{S}\int_0^S r(s) \sin \frac{n\pi s}{S}\, \mathrm{d}s, \tag{31, 32}$$

in which S is the total length of the contour.

The terms with $n = 1$ in equation (30) corresponds to the mass unbalances. The terms with $n = 2$ lead to different stiffness in different directions. The terms with $n > 2$ can almost always be neglected.

4.1. CHANGE OF THE IMPERFECTION ANGLE, φ, FOR CONSTANT VALUES OF THE FILAMENT WINDING ANGLE, α

The purpose of these analyses is to see how the geometry due to dynamic forces is effected by an imperfection. Two variables in Figure 4 have been varied, the filament winding angle, α, and the imperfection angle, φ. To see if these influence the behavior in any different manner, both will be studied.

Let the fibre orientation of the beam in Figure 4 change from $\alpha = 45^\circ$ to $\alpha = 42^\circ$ when $\varphi = 100^\circ$. The beam rotates at 20 000 r.p.m. and has a density, ρ, equal to 1382 kg/m^3.

The radius from the ABAQUS analysis, upon using equations (31) and (32), becomes

$$r = R[1{\cdot}00086 + (0{\cdot}0 \cos\theta - 12{\cdot}6 \sin\theta + 6{\cdot}0 \cos 2\theta - 0{\cdot}0 \sin 2\theta + \cos 3\theta - 1{\cdot}0 \sin 3\theta + \cdots)10^{-6}]. \tag{33}$$

It has been shown earlier in this section that the only terms in the Fourier series that substantially influence the eigenfrequencies are a_2 and b_2. The first terms (a_1 and b_1), however, move the mass center from the axis of rotation. This unbalance leads to an excitation force. In Figure 5, it is shown how the radius ratio $(R_0 - R)/R$ changes as a function of φ with $\alpha = 42^\circ$. From Figure 5, it is noted that the radius ratio $(R_0 - R)/R$ increases linearly from the radius of the beam without imperfections and the filament winding angle, α, equals 45° to the radius of a beam when α equal to 42°.

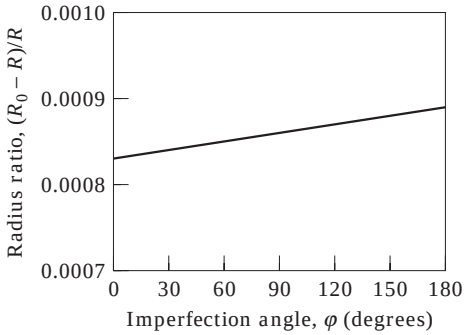

Figure 5. The radius ratio $(R_0 - R)/R$ of a composite beam versus the angle φ. The thickness-to-radius ratio (t/R) is 0·04, the rotational speed, Ω, is 20 000 r.p.m. and the density, ρ, is 1382 kg/m^3.

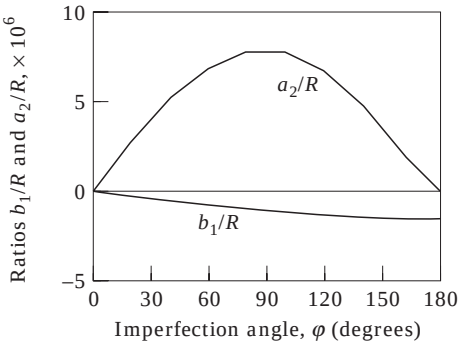

Figure 6. The ratios b_1/R and a_2/R versus the imperfection angle φ. The thickness-to-radius ratio (t/R) is 0·04, the rotational speed, Ω, is 20 000 r.p.m. and the density, ρ, is 1382 kg/m^3.

In Figure 6, it is shown how b_1 and a_2 change as a function of φ with $\alpha = 42^\circ$. Due to symmetry the terms a_1 and b_2 become zero in all analyses. From Figure 6, it is noted that the first sine term b_1 has largest influence when the two halves of the beam have different filament winding angles. The second cosine term a_2 has its largest influence when a quarter of the beam has a different filament winding angle.

4.2. DIFFERENT CHANGE OF FILAMENT WINDING ANGLE, α, WHEN $\varphi = 100^\circ$

In Figure 7, it is shown how the radius ratio $(R_0 - R)/R$ changes as a function of the filament winding angle α with $\varphi = 100^\circ$. From Figure 7, it is noted that the radius ratio $(R_0 - R)/R$ decreases linearly from the radius of the beam with an imperfection with the filament winding angle, α, equal to 35° to the radius of a beam with α equal to 55°.

In Figure 8, it is shown how b_1 and a_2 change as a function of α with $\varphi = 100^\circ$. Due to symmetry, the terms a_1 and b_2 become zero in the analyses. From Figure 8, it is noted that an imperfection with the filament winding angle smaller than 45° but higher than 35–40° has a limited effect on the two Fourier series terms.

4.3. EFFECTS ON EIGENFREQUENCIES

So far, the geometric changes due to imperfections have been studied. These effects have influence on the stress conditions. They also have influences on the performance of the rotor. It is obvious that if high precision is required these geometric changes have to be

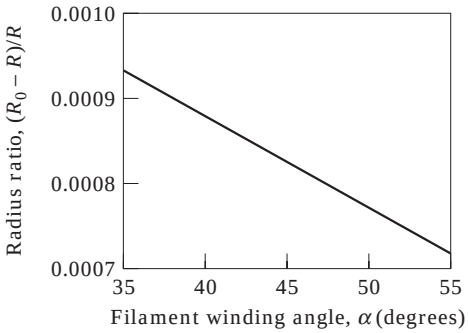

Figure 7. The radius ratio $(R_0 - R)/R$ for a composite beam versus the filament winding angle, α, with $\varphi = 100^\circ$. The thickness-to-radius ratio (t/R) is 0·04, the rotational speed, Ω, is 20 000 r.p.m. and the density, ρ, is 1382 kg/m^3.

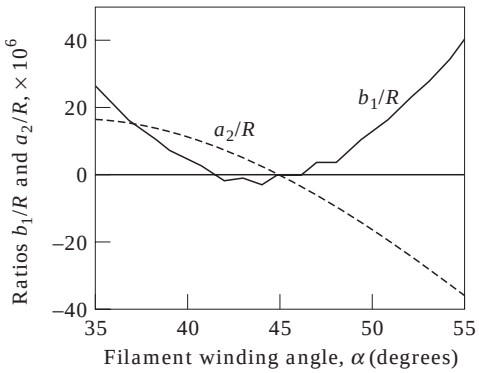

Figure 8. The ratios b_1/R and a_2/R versus the filament winding angle α with $\varphi = 100^\circ$. The thickness-to-radius ratio (t/R) is 0·04; the rotational speed, Ω, is 20 000 r.p.m.

small. Of great importance is the rotor vibration and the dynamic behavior of the rotor. Apart from the influence from the geometric changes the behavior also depends on the change in the stiffness due to the changes in the elastic modulus of the rotor.

In Table 2, the effect of the eigenfrequencies due to imperfections can be seen. The constant ω_0 is the angular frequency for the non-rotating shaft without imperfections. When $n = 0$ r.p.m. the geometry remains unchanged and the eigenfrequencies depend only on the material stiffness. When $n = 20\,000$ r.p.m. the eigenfrequencies also depend on the new geometry. The table also shows how the estimated eigenfrequencies depend on how many terms the Fourier series has. The effects of the imperfections on the eigenfrequencies have been plotted as a function of φ and α. This effect when $\alpha = 42^\circ$, with and without the geometric change due to the imperfection, is shown in Figure 9. The changes in the stiffness have the largest influence on the eigenfrequencies for different imperfection angles. The effects from geometric changes do not seem to affect the eigenfrequencies. In Figure 9, it is shown how the eigenfrequencies are affected when $\varphi = 100^\circ$ with different α, both with and without the geometric change due to the imperfection. Also, for different filament winding angles the changes in the stiffness have the largest influence on the eigenfrequencies. The affects from geometric changes do not seem to effect the eigenfrequencies.

The broken lines in Figures 9 and 10 are valid for the case in which the geometric changes have been excluded in the analysis, and the solid lines when the geometric changes have been included.

TABLE 2

The influence of Δr and n on ω_x/ω_0 (upper value) and ω_y/ω_0 (lower value) when $t/R_0 = 0{\cdot}04$ and $R_0/l = 0{\cdot}05$; the eigenfrequencies are affected by a change in the filament winding angle from $\alpha = 45^\circ$ to $\alpha = 42^\circ$ under $\varphi = 100^\circ$

Terms included	$n = 0$ rpm	$n = 20\,000$ rpm
$R_0, a_1, b_1, a_2, b_2, a_3, b_3$	0·9673 0·9916	0·9681 0·9924
R_0, b_1, a_2	0·9673 0·9916	0·9681 0·9924
R_0, a_2	0·9673 0·9916	0·9681 0·9924

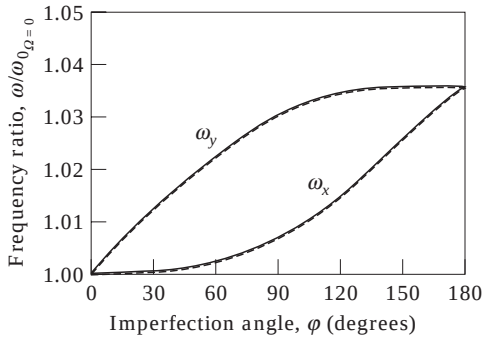

Figure 9. The frequency ratio versus the imperfection angle, φ. The filament winding angle changes from 45° to 42° in this example. The rotational speed is $\Omega = 20\,000$ r.p.m. and the density, ρ, is 1382 kg/m^3. ——, With geometric changes; —, without geometric changes.

4.4. DIFFERENT FILAMENT WINDING ANGLE

The major purpose of a drive shaft is to transmit a certain power at given speed. Most shafts are therefore designed to be able to transmit the required torque, which leads to an optimal filament winding angle close to 45°. Of course, there exist rotors where the optimal filament winding angle is different. For instance, a rotor where the lateral deflection is dimensioning has an optimal filament winding angle close to 15°. The filament winding angle is not normally the same in all layers. The same analyses as described so far in this section have been carried out for all filament winding angles. This means that $1^\circ < \alpha < 90^\circ$. In these analyses, $\varphi = 100^\circ$ in all cases. In Figure 11, the influence on R_0 is shown. From Figure 11, it is noted that the radius ratio $(R_0 - R)/R$ decreases from the radius of the beam with a filament winding angle $\alpha = 1^\circ$ to the radius of a beam with $\alpha = 90^\circ$. As was expected, fibres wound perpendicular to the axis of the mandrel, $\alpha = 90^\circ$, are least affected of the rotational speed, but fibre orientated by this angle can withstand only small longitudinal forces, which means that the lateral eigenfrequency becomes low.

In Figure 12, the influences on b_1 and a_2 are shown. It is noted in Figure 12 that the ratio b_1/R has extreme values when the filament winding angle, α, is 30° and 55° in the imperfectioned area. The ratio a_2/R has extreme values when α is 25° and 50°. These geometric and stiffness changes give the eigenfrequencies ratio shown in Figure 13. In this figure the eigenfrequencies are normalized to the maximum eigenfrequency in the interval for the shaft with imperfection, $\omega_{0,max_{with\ imperfection}}$. The eigenfrequencies ω_x and ω_y are the

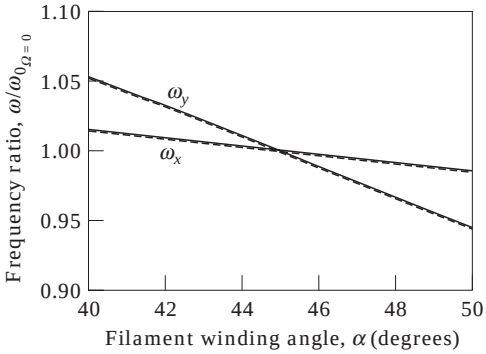

Figure 10. The frequency ratio versus the filament winding angle, α, when $\varphi = 100^\circ$. The rotational speed is $\Omega = 20\,000$ r.p.m. Key as Figure 9.

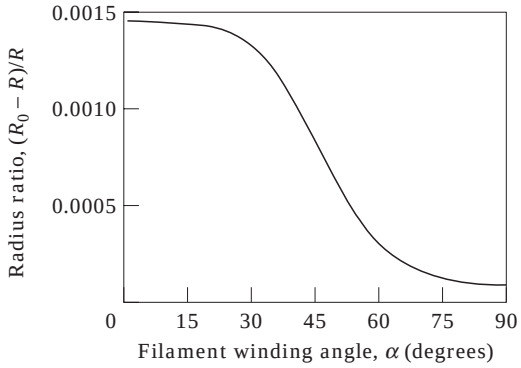

Figure 11. The radius ratio $(R_0 - R)/R$ for a composite beam versus the filament winding angle, α, with $\varphi = 100^\circ$. The thickness-to-radius ratio (t/R) is 0·04, the rotational speed, Ω, is 20 000 r.p.m. and the density, ρ, is 1382 kg/m^3. $\Delta\alpha = 1^\circ$.

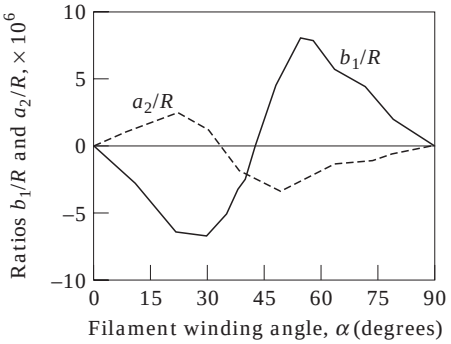

Figure 12. The ratios b_1/R and a_2/R versus the filament winding angle, with $\varphi = 100^\circ$. The thickness to radius ratio (t/R) is 0·04, the rotational speed, Ω, is 20 000 r.p.m. and the density, ρ, is the 1382 kg/m^3. $\Delta\alpha = 1^\circ$.

eigenfrequencies in the x and y directions, respectively. It is noted in Figure 13 that the frequency ratio has its optimum when the filament winding angle is approximately 15°. The difference between the two lines in Figure 13 appears more clearly if the variation of the difference $|\omega_y - \omega_x|/\omega_0$ is plotted. This has been done in Figure 14. In this figure the

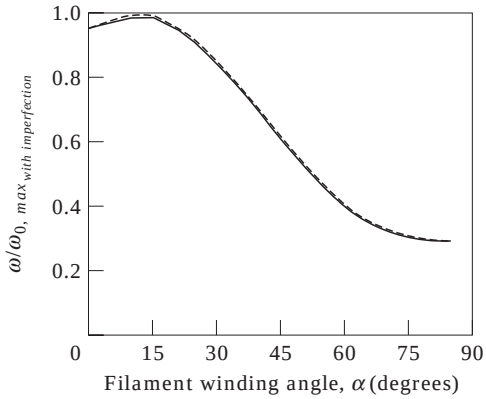

Figure 13. The frequency ratios versus the filament winding angle, with $\varphi = 100^\circ$. The rotational speed, Ω, is 20 000 r.p.m. and the density, ρ, is 1382 kg/m^3. ——, ω_x; ——, ω_y. $\Delta\alpha = 1^\circ$.

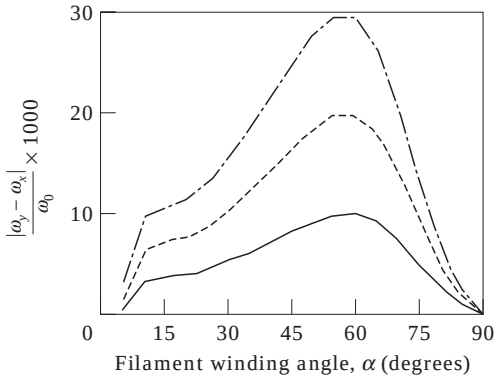

Figure 14. The normalized eigenfrequency ratio versus the filament winding angle, α. The thickness to radius ratio (t/R) is 0·04, the rotational speed, Ω, is 20 000 r.p.m. and the density, ρ, is 1382 kg/m^3. ——, $\Delta\alpha = 1^\circ$; · · · ·, $\Delta\alpha = 2^\circ$; –· –, $\Delta\alpha = 3^\circ$.

filament winding angle changes from α to $\alpha - \Delta\alpha$ with $\varphi = 100^\circ$, where $\Delta\alpha$ is 1°, 2° or 3°. From Figure 14, it is noted that the rotor has different eigenfrequencies in the x and y directions. In the interval $\omega_x < \Omega < \omega_y$, the rotor is unstable. In Figure 14, it is shown that this interval is smallest when the filament winding angle is as small as possible. The stiffness of the shaft will also be highest in this region (see Figure 13).

A comparison of Figures 10 and 14 shows that when the deviation from the main filament winding angle increases, the affect on $|\omega_y - \omega_x|/\omega_0$ also increases, in any case if $\alpha = 45^\circ$, and this seems to be valid for all values of α according to Figure 14.

5. STIFFENING OF A BEAM WITH LOCAL IMPERFECTION

An important issue is to investigate how a local imperfection may be stiffened by the surroundings. To study these phenomena the same type of beam as in Figure 4 has been used, but the beam is now stiffened by two beams without imperfections (see Figure 15). This beam will be called "beam with local imperfection". The total lengths of the beams are the same. The part marked with lines in Figure 15 has a filament winding angle different from the other part. The width of the imperfection area is defined by the imperfection angle φ, described in Figure 4.

The deformation of the middle of the middle beam due to centrifugal forces has been analyzed using the FEM program ABAQUS. A total of 108 elements of the type S8R5 have been used for modelling the beam.

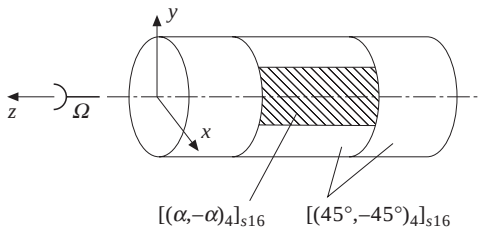

Figure 15. The three composite cylindrical parts have filament winding angle 45°. The middle shell, however, has a region with different filament winding angle.

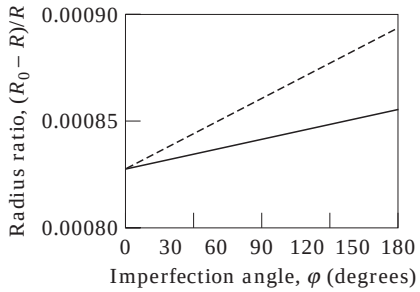

Figure 16. The radius ratio $(R_0 - R)/R$ versus the imperfection angle, φ. The thickness to radius ratio (t/R) is 0·04, the rotational speed, Ω, is 20 000 r.p.m. and the density, ρ, is 1382 kg/m^3. – –, Global imperfection; ——, local imperfection.

5.1. CONSTANT CHANGE OF FIBRE ORIENTATION, α, OVER φ DEGREES

The effects due to centrifugal forces for the rotational speed, Ω, equal to 2000 r.p.m. and the density, ρ, equal to 1382 kg/m^3 are shown in Figure 16. The radius ratio $(R_0 - R)/R$ changes as a function of φ with $\alpha = 42^\circ$, where R_0 is the first term in equation (1). As in all calculations in this paper, the radius, R, is equal to 0·05 m. From Figure 16 it is noted that $(R_0 - R)/R$ increases linearly from the radius of the beam without imperfections and the filament winding $\alpha = 45^\circ$ to the radius of a beam when $\alpha = 42^\circ$. The influence is not as large for the local imperfection as it is for the global imperfection.

In Figure 17, it is shown how b_1 and a_2 change as a function of φ. The filament winding angle, α, is equal to 42° in the imperfect area. From Figure 17, it is noted that the first sine term b_1 has largest influence when the two halves of the beam have different filament winding angles. The second cosine term, a_2, has its largest influence when a quarter of the beam has a different filament winding angle. It can also be seen that both the first sine term, b_1, and the second cosine term, a_2, have larger influence when the imperfection is local.

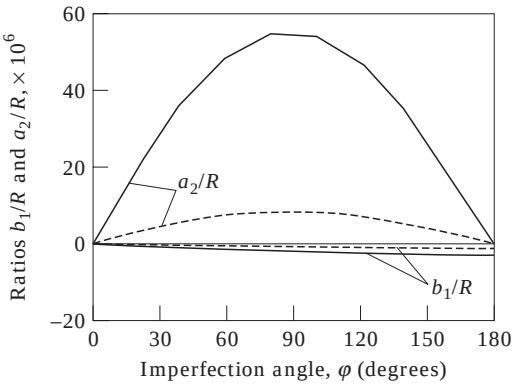

Figure 17. The first sine term, b_1, and second cosine term, a_2, in the Fourier series for a composite beam. The filament winding angle changes from $\alpha = 45^\circ$ to $\alpha = 42^\circ$ in the region with φ°. The thickness-to-radius ratio (t/R) is 0·04, the rotational speed, Ω, is 20 000 r.p.m. and the density, ρ, is 1382 kg/m^3. – – – –, Global imperfection; ——, local imperfection.

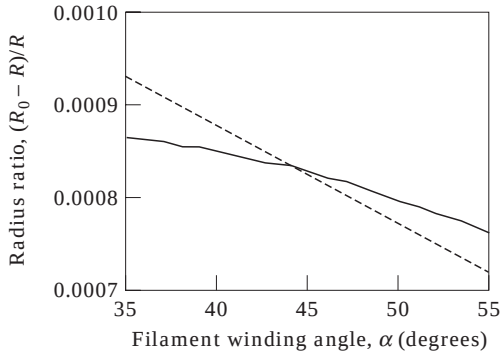

Figure 18. The radius ratio $(R_0 - R)/R$ versus the filament winding angle, α. The thickness-to-radius ratio (t/R) is 0·04, the rotational speed, Ω, is 20 000 r.p.m. and the density, ρ, is 1382 kg/m^3. ——, Global imperfection; ——, local imperfection.

5.2. CHANGE OF THE IMPERFECTION ANGLE, φ, FOR CONSTANT VALUES OF THE FILAMENT WINDING ANGLE, α

The same analyses as above have been carried out for a shaft with variation of filament winding angle. In Figure 18, it is shown how R_0 changes as a function of α with $\varphi = 100^\circ$ in the imperfect area. From Figure 18, it is noted that the base radius, R_0, for the beam with a local imperfection is not affected as much as a shaft with a global imperfection. This was, of course, expected. In both cases the radius ratio $(R_0 - R)/R$ decreases almost linearly from the radius of the beam with an imperfection with the filament winding angle, α, equal to 35° to the radius of a beam with α equal to 55°. In Figure 19, it is shown, however, that the second cosine term for a local imperfection is the term most affected by the imperfection. This phenomenon may depend on the constraint imposed by stiffening with beams. The first sine term is almost the same for a local and a global imperfection.

5.3. EFFECTS ON EIGENFREQUENCIES

The geometrical and stiffness changes gives the eigenfrequencies shown in Figure 20. In this figure ω_0 is the eigenfrequency for a beam without imperfections. As can be expected, the greater the deviation from $\alpha = 45^\circ$ the more the eigenfrequency differs from the value it had without imperfections.

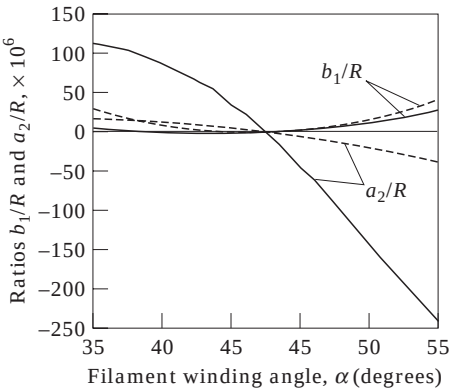

Figure 19. The ratios b_1/R and a_2/R versus the filament winding angle in the region in which $\varphi = 100^\circ$. The thickness-to-radius ratio (t/R) is 0·04; the rotational speed, Ω, is 20 000 r.p.m. ——, Global imperfection; ——, local imperfection.

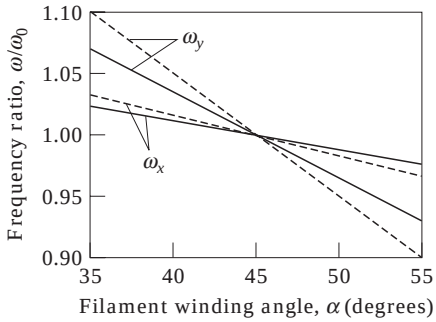

Figure 20. The frequencies ratio versus the filament winding angle, α. Thickness-to-radius ratio (t/R) is 0·04; the rotational speed, Ω, is 20 000 r.p.m. Key as Figure 19.

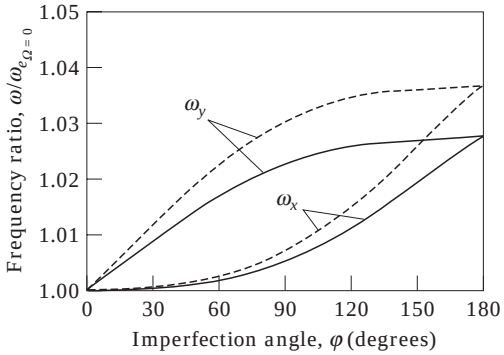

Figure 21. The frequency ratio versus the imperfection angle, φ. The filament winding angle changes from 45° to 42°. The rotational speed is 20 000 r.p.m. Key as Figure 19.

In Figure 21, it is shown how the eigenfrequencies depend on the imperfection angle. It is noted that the larger the part of the shaft is that has an imperfection, the more the eigenfrequency increases from the value that it had without imperfections.

The variation of the difference $|\omega_y - \omega_x|/\omega_0$ for different filament winding angles has been plotted in Figure 22. In Figure 22, it is shown that the influence of the imperfection in the region where the stiffness of the shaft is highest ($10° < \alpha < 15°$) is half as much as large if the imperfection had been stiffened. Unfortunately, the maximum influence appears when the filament winding angle, α, is 45°. Most shafts have this filament winding angle,

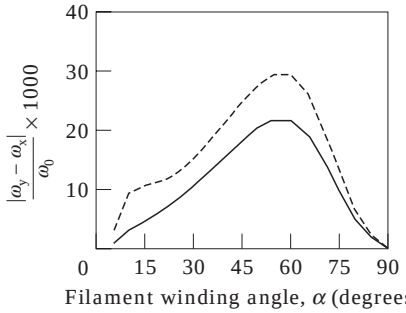

Figure 22. The frequency ratio versus the filament winding angle, α, over $\varphi = 100°$. The thickness-to-radius ratio (t/R) is 0·04; the rotational speed, Ω, is 20 000 r.p.m. ——, Global imperfection; ——, local imperfection.

because the dominant failure mechanism for torsionally loaded shafts is torsional buckling (see reference [8]).

6. CONCLUSIONS

Due to centrifugal forces, imperfections in thin-walled shafts will lead to changes in the geometry. The behavior of the shaft is therefore different at different rotational frequencies. From the results in this paper, the following conclusions can be drawn.

The difference between the eigenfrequencies in the two perpendicular directions, x and y, due to the second term in a Fourier expansion of the radius is almost proportional to the radius. The influence on the eigenfrequency from the other terms increases more than linearly, but their absolute value is normally negligible compared to that of the second term.

The term $\Delta\omega_{n=2}$ is almost proportional to Δr. The influence on the eigenfrequency from the other terms increases more than linearly; however, their absolute value is normally negligible compared to that when $n = 2$.

When the rotor is non-rotating, the geometry remains unchanged and the eigenfrequencies depend only on the material stiffness. When $n = 20\,000$ r.p.m., the eigenfrequencies also depend on the new geometry. The difference between these two cases is negligible, which means that the change in the stiffnesses has much greater influence than the change in the geometry.

The effect on the eigenfrequency of a local imperfection is of the same kind as for a global imperfection, except that the influence is smaller.

Imperfections of the types described in this paper have the largest influence when the filament winding angle is about 60°.

The conclusion must be that the influences of filament winding imperfections are small, but they may be one explanation of why there are such difficulties in using composite shafts in supercritical applications, since a rotor becomes unstable in the region of the eigenfrequency when the shaft has an asymmetry. Another consequence of the imperfection may be that the shafts subjected to centrifugal forces get an extra bow which may increase (or decrease) the effects of an imbalance. This may be the explanation of why Zorzi and Giordano [1] observed that the composite shafts tested showed greater sensitivity to imbalance than the aluminum control shaft.

REFERENCES

1. E. S. Zorzi and J. C. Giordano 1985 *Paper presented at the ASME Design Engineering Division Conference and Exhibition on Mechanical Vibration and Noise*, *Cincinnati*, *Ohio*, 10–13 *September*. Composite shaft rotordynamic evaluation.
2. O. A. Bauchau 1981 *Ph.D. Thesis*, *Department of Aeronautics and Astronautics*, *MIT*. Design, manufacturing and testing of high speed rotating graphite/epoxy shafts.
3. O. A. Bauchau 1983 *Journal of Composite Materials* **17**, 170–181. Optimal design of high speed rotating graphite/epoxy shafts.
4. ASM International Committee 1987 *Engineered Materials Handbook*, Volume 1, U.S.A.
5. X. X. Wu and C. T. Sun 1989 *Vibration and Behavior of Composite Structures*, Volume 14. New York: The American Society of Mechanical Engineers. See pp. 47–52. Vibration of thin-walled composite structures.
6. H. L. Wettergren, 1996 *Ph.D. Thesis. Linköping University*, *Department of Mechanical Engineering*, *Sweden*. Rotordynamic analysis with special reference to composite rotors and internal damping.
7. S. W. Yurgartis 1987 *Composite Science and Technology* **30**, 279–293. Measurement of small angle fiber misalignments in continuous fiber composites.

8. J. Creonte and M. S. Darlow 1992 *Proceedings of the IMechE Conference on Vibrations in Rotating Machinery*, *Bath*, 7–10 *September*, 149–154. Optimal design of supercritical, composite shafts with axially varying fibre lay-up.